Electronic Supplementary Information

Unveiling the dimension dependence of femtosecond nonlinear optical properties of tellurium nanostructures

Qi Xiao,[a] Bo Ma,[a] Xian Fei,[a] Duan-Wu Liu,[a] Xin-Ping Zhai,[a] Xiang-Yang Li,[a] Ming-Jun Xiao,[a] Yong Peng,[b] Qiang Wang[a] and Hao-Li Zhang*[a, c]*

a State Key Laboratory of Applied Organic Chemistry, Key Laboratory of Special Function Materials and Structure Design, College of Chemistry and Chemical Engineering, Lanzhou University, Lanzhou, 730000, P. R. China.

b Key Laboratory of Magnetism and Magnetic Materials of MOE, Lanzhou University, Lanzhou, 730000, P. R. China.

c Tianjin Key Laboratory of Molecular Optoelectronic Sciences, Department of Chemistry, Tianjin University, Collaborative Innovation Center of Chemical Science and Engineering (Tianjin), Tianjin 300072, P. R. China.

Experimental Procedures

Materials. Tellurium (Te) crystal was purchased from Alfa Aesar (99.9999%). 2-butanol, N-methyl pyrrolidone (NMP), isopropanol (IPA), acetone, ethanol and H_2SO_4 were purchased from Rionlon Bohua (Tianjin) Pharmaceutical & Chemical Co. Ltd. NaCl, LiCl, Na_2SO_4, $NaNO_3$ and K_2SO_4 were purchased from Tianjin Chemical Reagent Factory (China). Ultrapure water was obtained with a Milli-Q System (Billerica, MA, U.S.).

Electrochemical exfoliation. In a typical exfoliation process, the Te crystal with the size of 1 cm × 0.5 cm connected by a copper clip worked as cathode. A Pt wire was used as counter-electrode, which was fixed in parallel to Te electrode at the distance of 1 cm. The electrochemical exfoliation of Te immediately occurred by applying 10 V bias on Te electrode. After 10 mins exfoliation, the products were collected and washed with deionized water 5 times. Then the samples were re-dispersed in NMP via mild sonication for 30 min and centrifuged at 1,500 rpm for 10 minutes to remove the unexfoliated bulk. Finally, the supernatant was taken out for further measurement and characterization.

Liquid phase exfoliation (LPE). The bulk Te crystals were broken into small pieces, and ball-milled at 500 rpm for 1 h in stainless steel vials (100 mL each) with stainless steel balls (5, 8 and 10 mm in diameter, total weight of 140 g) on a planetary ball mill (Changsha Deco) under an ambient atmosphere. Then the resulted Te micro-crystals were dispersed in 2-butanol with ice-bath sonication for 3 h. Finally, the dispersions were centrifuged at 3,000 rpm for 3 min, and the supernatant was collected for further measurement and characterizations.

Characterization. The UV-Vis-NIR absorption spectra were obtained on a TU-1810 spectrophotometer (Beijing Purkinje General Instrument, China). Raman spectra were carried out on a confocal microscope Raman system (Renishaw in via Raman microscope) excited by 633 nm laser. Powder X-ray diffraction (PXRD) patterns of the products were recorded on a

PANalytical X'Pert PRO powder diffractometer using Cu Kα radiation (λ = 1.5418 Å). X-ray photoelectron spectroscopy (XPS) was measured by AXIS Ultra using monochromatized Al Kα X-ray photons. The transmission electron microscopic (TEM) images and scanning transmission electron microscopy-energy dispersive X-ray spectroscopic (STEM-EDX) were acquired on a FEI Talos F200S Field Emission Transmission Electron Microscope at operating voltages of 200 kV. The scanning electron microscope (SEM) micrographs were obtained using field-emission scanning electron microscopy (FE-SEM, Hitachi S4800) at an accelerating voltage of 2.0 kV. Atomic Force Microscope (AFM) was carried out on Agilent 5500.

Femtosecond (fs) transient absorption (TA) spectroscopy. The laser source was a Coherent Legend Elite regenerative amplifier (<110 fs, 1 KHz, 800 nm), seeded by a Coherent Chameleon oscillator (75 fs, 80 MHz). Pump laser at 400 nm were acquired by doubling the fundamental 800 nm pulses with a BBO crystal. The white probe pulses in 330-600 nm range were generated on a CaF_2 crystal, which was excited by partial of the 800 nm laser beam from the amplifier. The data were fitted using Surface Xplore software (Ultrafast Systems, LLC). The nonlinear optical properties were measured by open-aperture Z-scan setup using the same fs laser source in fs TA experiments. The 532 nm and 600 nm laser were generated from a Light Conversion OPerA-Solo optical parametric amplifier (285-2600 nm).

Characterization

Fabrication of Te nanostructures

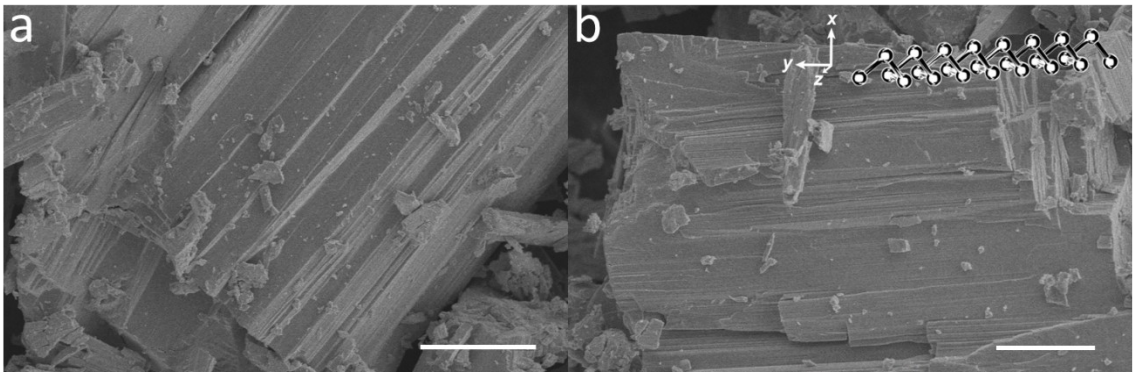

Figure S1. SEM images of bulk Te showing chain-like structure. Inset of (b) is the simulated Te chain. Scale bar, 20 μm (a); 10 μm (b).

Table S1. Summary of the exfoliation conditions of Te nanostructures

	Electrolyte	Bias voltage	Exfoliation time	Yield
Te nanodot (NDs)	0.5 M Na_2SO_4	-10 V	10 mins	902 mg
Te nanorod (NRs)	0.5 M H_2SO_4	-10 V	10 mins	785 mg
Te nanowire (NWs)	0.05 M H_2SO_4	-7 V	10 mins	76 mg

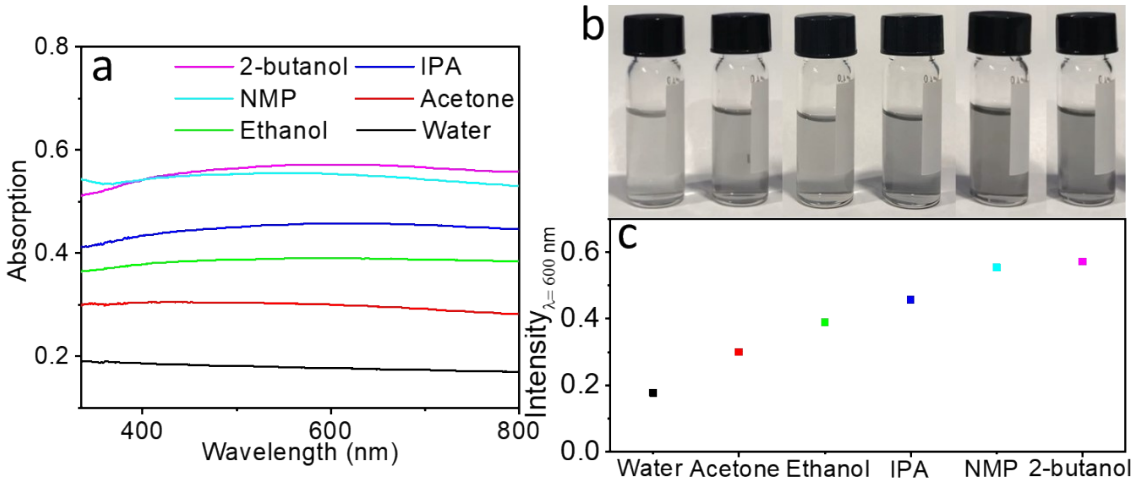

Figure S2. Solvent selection: a) Absorption spectra of 2D Te NSs exfoliated in water, acetone, ethanol, IPA, NMP and 2-butanol, respectively. b) The corresponding photographs of 2D Te NSs suspensions. c) Comparison of the absorption intensity at wavelength of 600 nm.

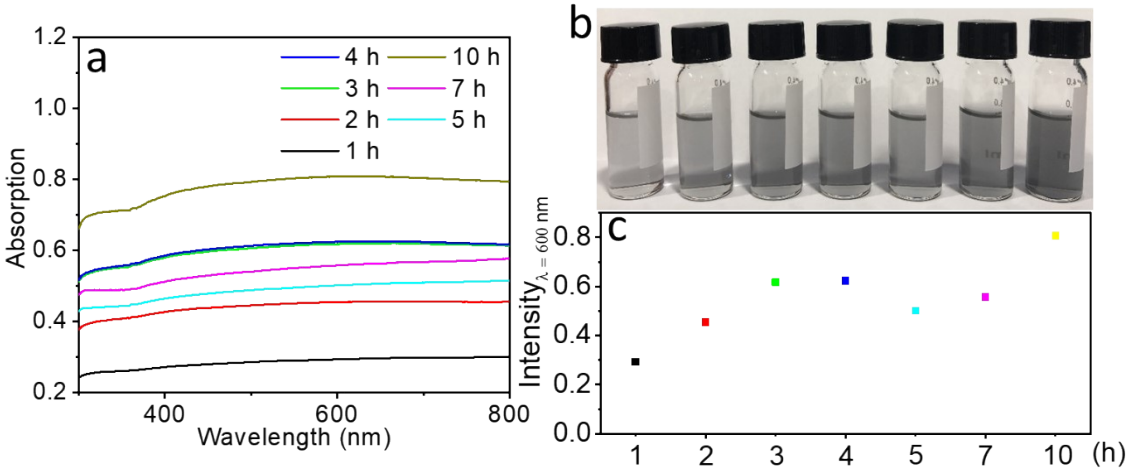

Figure S3. Optimization of sonication time: a) Absorption spectra of 2D Te NSs exfoliated in 2-butanol with increasing sonication time. b) The corresponding photographs of 2D Te NSs suspensions. c) Comparison of the absorption intensity at wavelength of 600 nm.

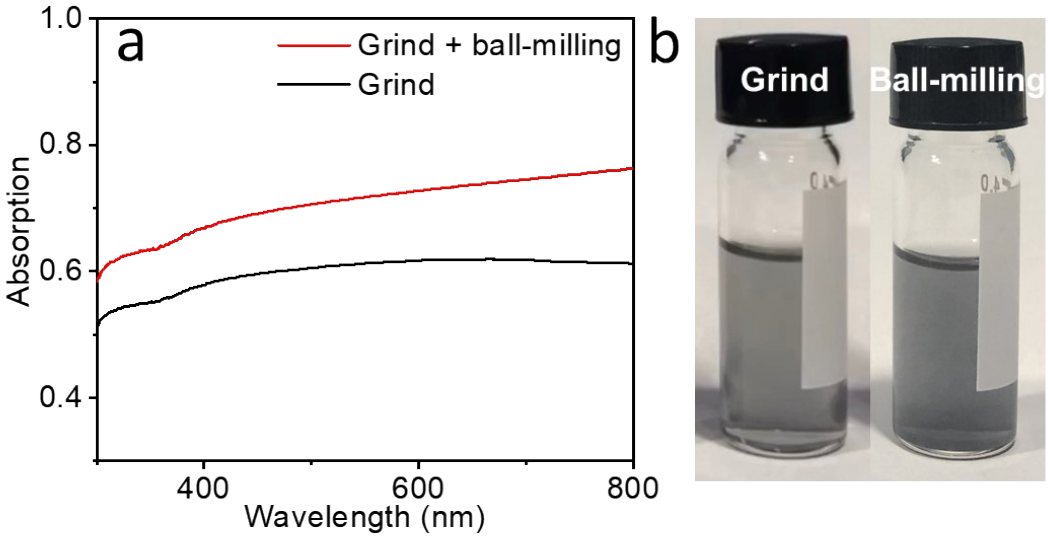

Figure S4. Optimization of pretreatment process: a) Absorption spectra of 2D Te NSs exfoliated in 2-butanol with different pretreatment process: only grind and grind + ball-milling. b) The corresponding photographs of 2D Te NSs suspensions.

The influences of different exfoliated parameters such as the pretreatment process, types of solvents and the sonication time on the efficiency of the exfoliation were systematically studied.

Figure S2a depicts absorption spectra of 2D Te NSs exfoliated in water, acetone, ethanol, IPA, NMP and 2-butanol, respectively. The gradually increasing absorption in these solvents indicating the increasing concentration of 2D Te, which can be easily seen in the corresponding optical images in Figure S2b. Figure S2c shows the comparison of the absorption intensity at wavelength of 600 nm. Previous reports indicated IPA[1] and NMP[2] is the good solvents for the exfoliation of Te. Here, 2-butanol is demonstrated to an even better solvent for Te exfoliation, probably because the Hansen solubility parameters of 2-butanol is 22.2 lower than that of IPA (23.5) and NMP (22.9).[3] Moreover, 2-butanol is a mild solvent, which will reduce the crystal damage during the LPE process.

Once the solvent is selected, other experimental parameter may influence the LPE process

of Te to form a stable dispersion, such as the sonication time. Figure S3a shows the absorption spectra of 2D Te NSs exfoliated in 2-butanol with sonication time of 1 h, 2 h, 3 h, 4 h, 5 h, 7 h, and 10 h, respectively. Interestingly, the absorption of 2D Te is not rising monotonously as the increase of sonication time, but the absorption gets a slightly decrease after 3 - 4 h sonication. The slightly decrease in absorption is shown more clearly in the optical images of Te dispersion (Figure S3b) and the comparison of the absorption intensity at wavelength of 600 nm (Figure S3c), which is also found in the previous report of Te exfoliation,[1] probably due to the greatly size reduction of Te NSs and the formation of Te oxides after long time sonication.

The pretreatment process is also proved to be an important factor that strongly influence the LPE process.[4, 5] Figure S4a shows the absorption spectra of 2D Te NSs dispersion produced under grind and ball-milling the bulk Te crystals before 3 h sonication in 2-butanol, and Figure S4b shows the corresponding photographs of these suspensions. The sample with ball-milling pretreatment shows a greatly increase in the absorption and darker color than the one only under grind pretreatment process, indicating the promoted yield and the superiority of ball-milling pretreatment. Finally, the optimal conditions of Te exfoliation were ball-milling pretreatment process matched with 3 h sonication in 2-butanol.

Characterization of Te nanostructures

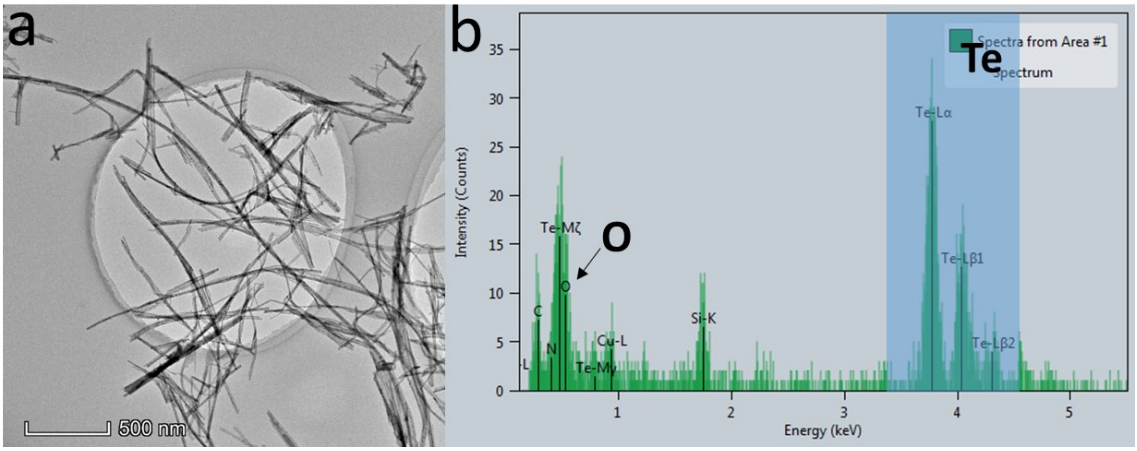

Figure S5. a) TEM image of Te NWs. b) Energy dispersive spectrometer (EDS) of Te NWs.

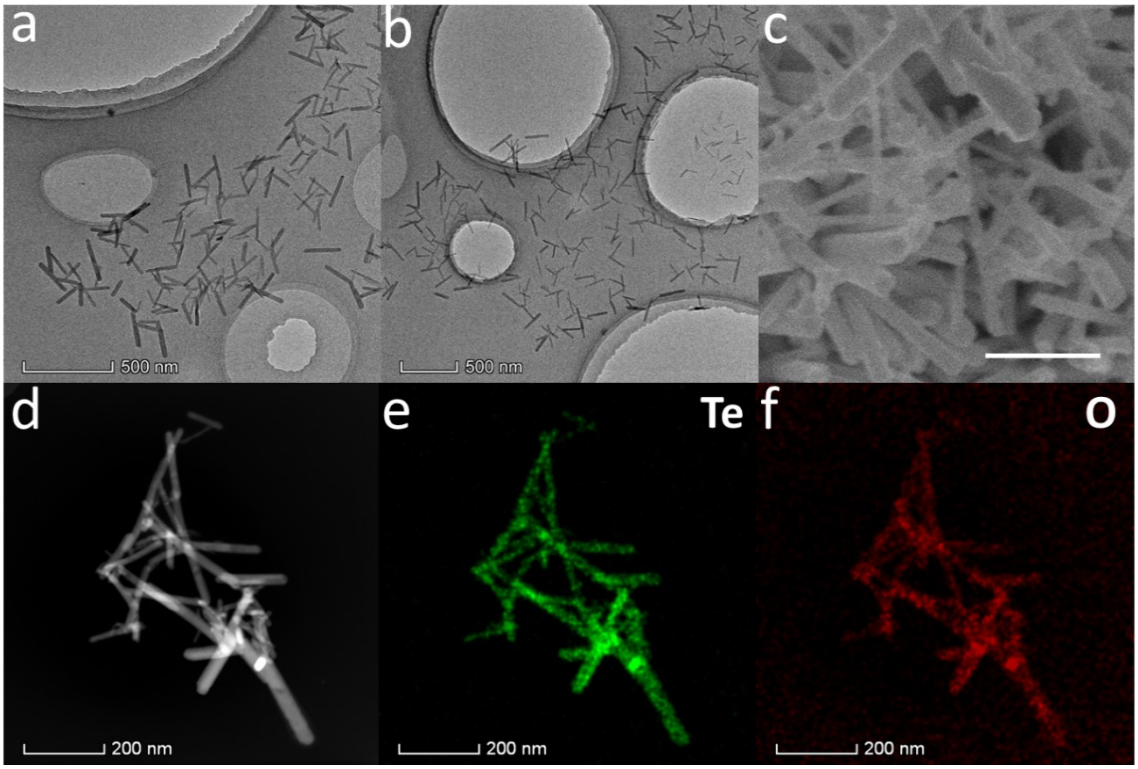

Figure S6. a, b) TEM images of Te NRs. c) SEM image of Te NRs. Scale bar: 200 nm. d)

High-angle annular dark-field (HAADF)-STEM image of Te NRs. e, f) Element mapping of Te and O elements, respectively.

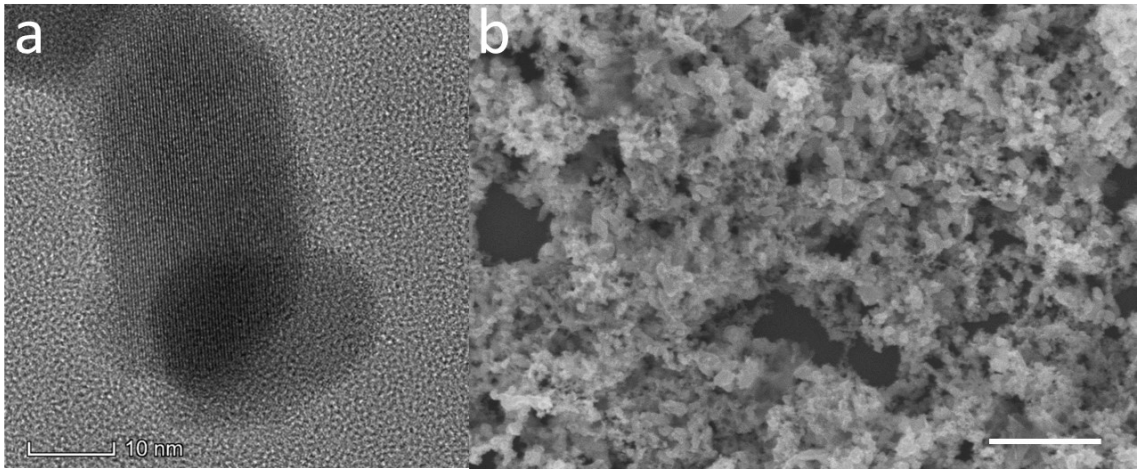

Figure S7. a) TEM image of Te NDs. b) SEM image of Te NDs. Scale bar, 500 nm.

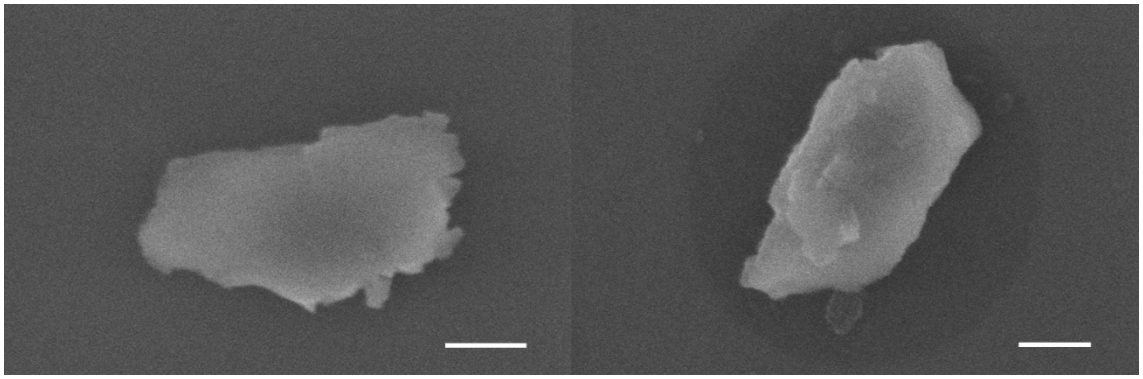

Figure S8. SEM images of Te NSs. Scale bar: 200 nm.

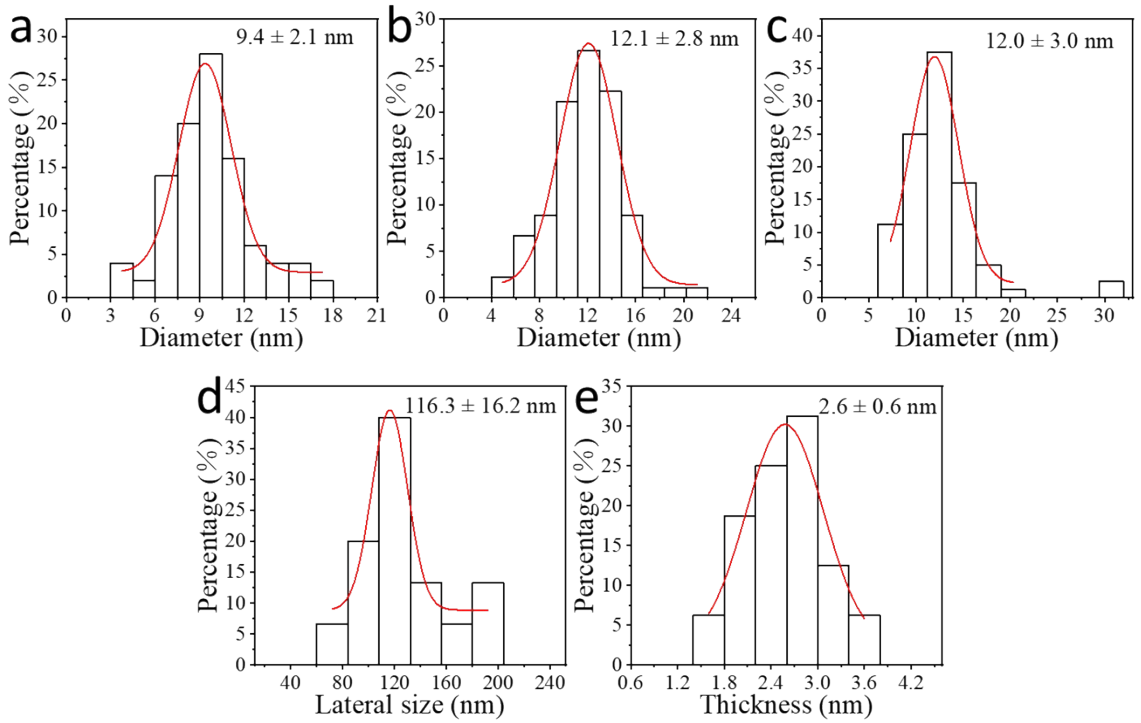

Figure S9. The statistical histogram of size distribution: The diameter distribution for a) Te NWs, b) Te NRs and c) Te NDs; d) lateral size distribution of Te NSs; e) thickness distribution of Te NSs. Each histogram represents the statistic results from near 100 samples to ensure accuracy.

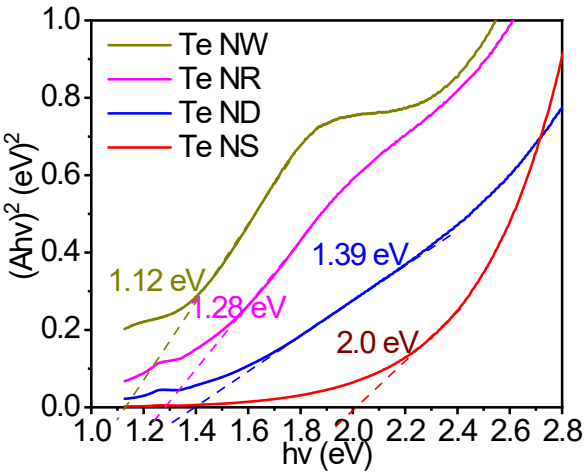

Figure S10. Tauc plots of Te NWs, NRs, NDs and Te NSs for calculations of band gap energies derived from the absorption spectra in Figure 3a.

Nonlinear optical measurement of Te nanostructures

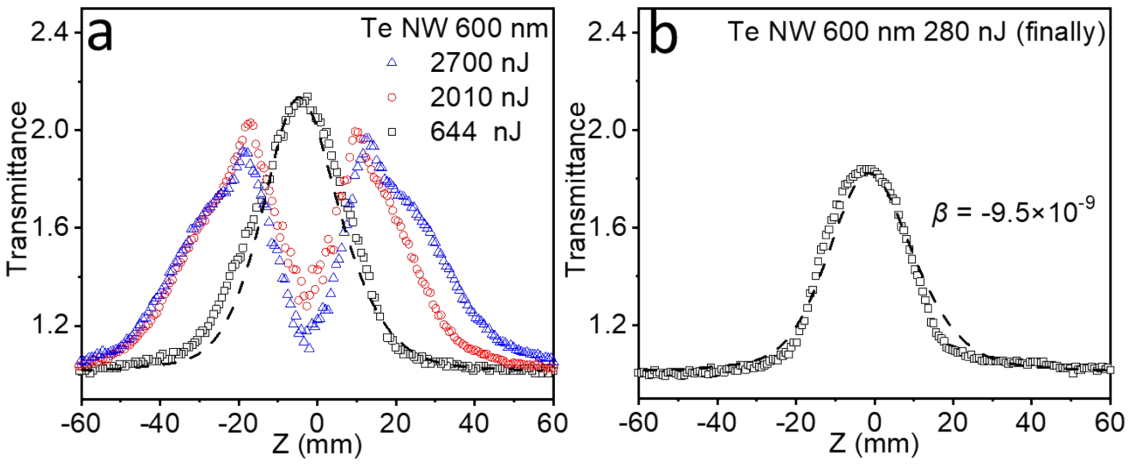

Figure S11. Fs open-aperture Z-scan results of the Te NWs. a) Experimental results of Te NWs under laser power of 644, 2010 and 2700 nJ. Dashed lines: fitted z-scan curves. b) Experimental results of the same Te NWs sample finally under laser power of 280 nJ (hollow squares) after the laser power increased to 2700 nJ. Dashed lines: fitted z-scan curves.

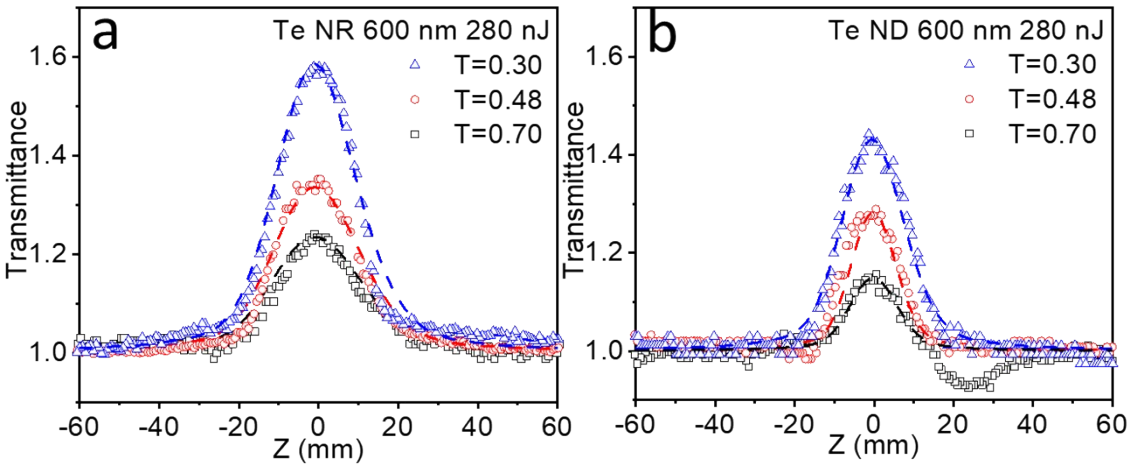

Figure S12. Fs open-aperture Z-scan results of the Te NRs and NDs. Experimental results of a) Te NRs and b) Te NDs with the sample transmittance of 0.7, 0.48 and 0.3. Dashed lines: fitted z-scan curves.

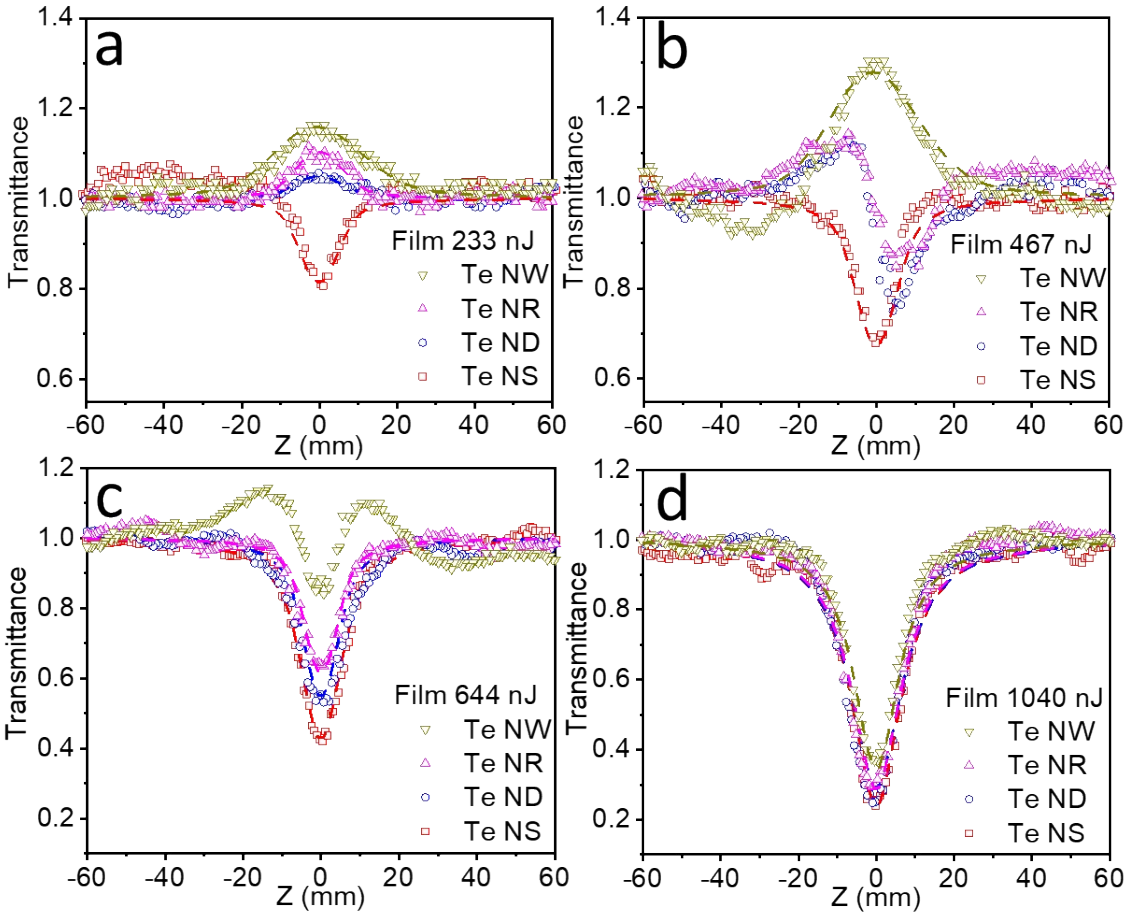

Figure S13. Experimental results of fs open-aperture Z-scan results of the Te/PMMA films (transmittance of 0.82) under excitation of 600 nm with laser intensities of a) 233 nJ, b) 467 nJ, c) 644 nJ and d) 1040 nJ. Dashed lines: fitted Z-scan curves.

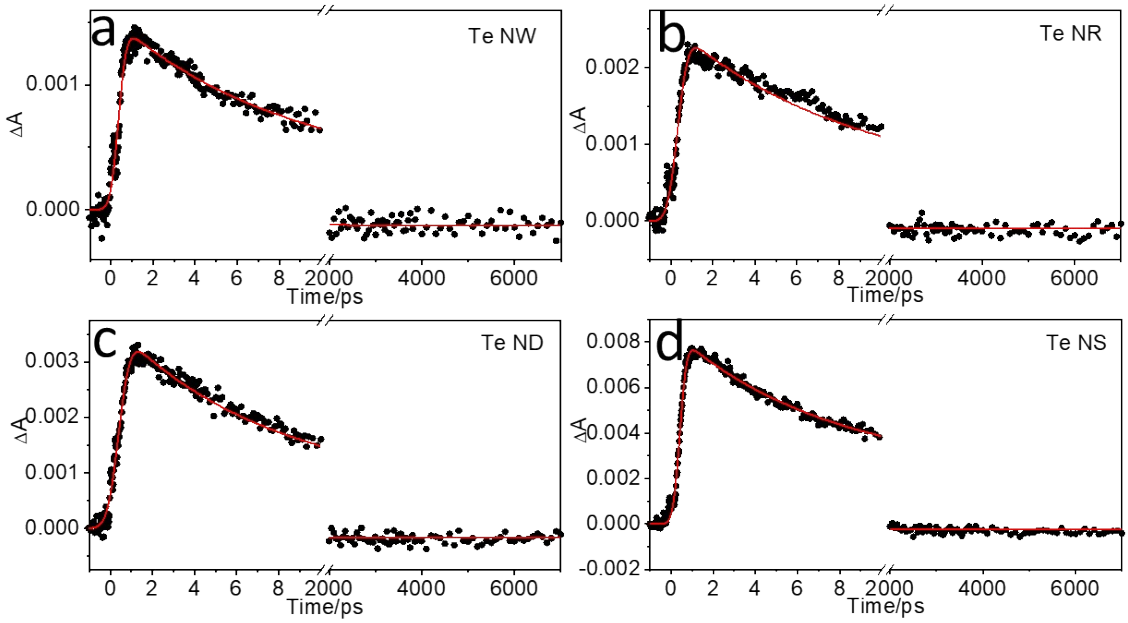

Figure S14. Experimental results of representative decay curves of a) Te NWs, b) Te NRs, c) Te NDs and d) Te NSs recorded at 780 nm (black solid circles) of fs transient absorption spectra, respectively. Red solid lines: fitted z-scan curves.

Table S2. Summary of the NLO parameters for Te nanostructures.

Materials	T (%)	Laser	β (m/W)
Te NWs	70.0	600 nm, 644 nJ	$-15.3 \pm 3.1\% \times 10^{-9}$
	70.0	600 nm, 280 nJ	$-9.8 \pm 6.1\% \times 10^{-9}$
	48.0	600 nm, 280 nJ	$-13.8 \pm 4.8\% \times 10^{-9}$
	30.0	600 nm, 280 nJ	$-21.8 \pm 4.6\% \times 10^{-9}$
	70.0	600 nm, 218 nJ	$-8.3 \pm 3.6\% \times 10^{-9}$
	70.0	532 nm, 862 nJ	$-3.8 \pm 2.0\% \times 10^{-9}$
Te NWs/PMMA	82.0	600 nm, 233 nJ	$-7.5 \pm 1.9\% \times 10^{-10}$
	82.0	600 nm, 467 nJ	$-9.5 \pm 1.9\% \times 10^{-10}$
Te NRs	70.0	600 nm, 280 nJ	$-6.8 \pm 2.6\% \times 10^{-9}$
	48.0	600 nm, 280 nJ	$-10 \pm 2.2\% \times 10^{-9}$
	30.0	600 nm, 280 nJ	$-16 \pm 1.4\% \times 10^{-9}$
	70.0	600 nm, 218 nJ	$-6.7 \pm 3.9\% \times 10^{-9}$
Te NRs/PMMA	82.0	600 nm, 233 nJ	$-3.5 \pm 6.1\% \times 10^{-10}$
	82.0	600 nm, 644 nJ	$4.5 \pm 4.5\% \times 10^{-9}$
Te NDs	70.0	600 nm, 280 nJ	$-2.5 \pm 3.6\% \times 10^{-9}$
	48.0	600 nm, 280 nJ	$-4.0 \pm 4.1\% \times 10^{-9}$
	30.0	600 nm, 280 nJ	$-7.4 \pm 5.0\% \times 10^{-9}$
	70.0	600 nm, 218 nJ	$-3.5 \pm 2.2\% \times 10^{-9}$
Te NDs/PMMA	82.0	600 nm, 233 nJ	$-1.9 \pm 7.6\% \times 10^{-10}$
	82.0	600 nm, 644 nJ	$5.8 \pm 5.0\% \times 10^{-9}$
Te NSs	70.0	600 nm, 218 nJ	$3.1 \pm 1.1\% \times 10^{-9}$
	70.0	532 nm, 862 nJ	$9.0 \pm 4.3\% \times 10^{-9}$
Te NSs/PMMA	82.0	600 nm, 233 nJ	$7.5 \pm 2.3\% \times 10^{-10}$
	82.0	600 nm, 467 nJ	$9.0 \pm 4.2\% \times 10^{-10}$
	82.0	600 nm, 644 nJ	$7.0 \pm 1.1\% \times 10^{-9}$

References

1. Z. Xie, C. Xing, W. Huang, T. Fan, Z. Li, J. Zhao, Y. Xiang, Z. Guo, J. Li, Z. Yang, B. Dong, J. Qu, D. Fan and H. Zhang, *Adv. Funct. Mater.*, 2018, **28**, 1705833.
2. L. Wu, W. Huang, Y. Wang, J. Zhao, D. Ma, Y. Xiang, J. Li, J. S. Ponraj, S. C. Dhanabalan and H. Zhang, *Adv. Funct. Mater.*, 2019, **29**, 1806346.
3. L. Zhang, S. Fahad, H. R. Wu, T. T. Dong, Z. Z. Chen, Z. Q. Zhang, R. T. Liu, X. P. Zhai, X. Y. Li, X. Fei, Q. W. Song, Z. J. Wang, L. C. Chen, C. L. Sun, Y. Peng, Q. Wang and H. L. Zhang, *Nanoscale Horiz.*, 2020, **5**, 1420.
4. X. Wang, J. Song and J. Qu, *Angew. Chem., Int. Ed.*, 2019, **58**, 1574.
5. Q. Xiao, C.-X. Hu, H.-R. Wu, Y.-Y. Ren, X.-Y. Li, Q.-Q. Yang, G.-H. Dun, Z.-P. Huang, Y. Peng, F. Yan, Q. Wang and H.-L. Zhang, *Nanoscale Horiz.*, 2020, **5**, 124.